

Federated Action Recognition on Heterogeneous Embedded Devices

Pranjal Jain*, Shreyas Goenka*, Saurabh Bagchi, Biplab Banerjee, Somali Chaterji

Abstract—Federated learning allows a large number of devices to jointly learn a model without sharing data. In this work, we enable clients with limited computing power to perform action recognition, a computationally heavy task. We first perform model compression at the central server through knowledge distillation on a large dataset. This allows the model to learn complex features and serves as an initialization for model fine-tuning. The fine-tuning is required because the limited data present in smaller datasets is not adequate for action recognition models to learn complex spatio-temporal features. Because the clients present are often heterogeneous in their computing resources, we use an asynchronous federated optimization and we further show a convergence bound. We compare our approach to two baseline approaches: fine-tuning at the central server (no clients) and fine-tuning using (heterogeneous) clients using synchronous federated averaging. We empirically show on a testbed of heterogeneous embedded devices that we can perform action recognition with comparable accuracy to the two baselines above, while our asynchronous learning strategy reduces the training time by 40% relative to synchronous learning.

Impact Statement—In order to enable edge devices to perform action recognition using limited computing power, we have developed a federated learning framework that also takes into account the heterogeneity of resources present on each embedded device. CCTV cameras, which are critical to security applications, often require the classification of abnormal activity. Since privacy is crucial, the video data cannot always be transferred to a central server. Hence, the training needs to occur at the edge devices themselves. In order to ensure that downtime on certain devices does not affect the rest of the system, in this paper, we use asynchronous updates. The framework in this paper can be used in a variety of applications, including, but not limited to, industry, defense and government applications.

Index Terms—Computer Vision, Action Recognition, Federated Learning, Edge Computing

I. INTRODUCTION

Action recognition has been a long-standing and actively pursued problem in the computer vision community due to its practical applications in areas such as surveillance, semantic video retrieval and multimedia mining. Video action recognition involves the identification of actions from video clips. This

may seem like an extension of image classification to multiple frames: predicting the action in each frame and aggregating the predictions. However, the success of image classification on datasets such as ImageNet [1] has not been replicated in video classification. Several challenges exist in video recognition such as huge computational costs, capturing long spatio-temporal contexts, and designing classification architectures. Human action recognition approaches can be categorized into visual sensor-based, non-visual sensor-based, and multi-modal categories [2], [3]. The main difference between visual and other categories is the form of the sensed data. The visual data are captured in the form of 2D/3D images or video whilst others capture the data in the form of a 1D signal [3].

Apart from fully-supervised methods [4], [5], [6], [7], several papers discuss few-shot [8], [9] mechanisms and zero-shot learning mechanisms [10], [11]. As the name suggests, in few-shot learning, the number of training examples is limited, and in zero-shot learning, we use test samples from classes that were not observed during training. The datasets available for the task have variable sizes; some such as the Kinetics [12] have sufficient data to train large models, whereas others like HMDB51 [13] and UCF101 [14] result in model overfitting due to limited data. We also empirically see here that ResNet training resulted in significant overfitting for UCF-101 and HMDB-51 but not for Kinetics [15]: ResNet-18 trained from scratch on HMDB51 achieved a per-clip accuracy of 17.1% whereas a model pretrained on the Kinetics dataset and fine-tuned on HMDB51 achieved a per-clip accuracy of 56.4% [16]. As datasets grow in size and complexity, an additional limiting factor is that of constraints such as computation, time required, and costs associated with training [17]. These constraints become crucial in edge devices, which typically have limited computation and storage and unpredictable network connectivity to a central server [18]. Limited device storage in turn implies that clients can accommodate only small local datasets, and as seen in previous work [16], this results in inaccurate models.

Although computer vision algorithms have achieved high accuracy on several tasks, it comes at the price of large computational costs [19]. Federated learning aims to leverage the computing power and data of a multitude of clients, often with significant heterogeneity in terms of computational power and network bandwidth, to build models. Federated learning is also motivated by the desire for privacy preservation [20], eliminating the risk of sensitive data transfer to a central server [21], [22], [23]. Furthermore, the technique is most often implemented using the synchronous approach, which assumes that clients proceed in lockstep. Particularly in our

*Pranjal Jain and Shreyas Goenka contributed equally to this paper.

Pranjal Jain is with the Electrical Engineering Department, Indian Institute of Technology Bombay, Mumbai, India (email: pranjal0000@gmail.com).

Shreyas Goenka is with the Electrical Engineering Department, Indian Institute of Technology Bombay, Mumbai, India (email: shreyasgoenka7@gmail.com).

Saurabh Bagchi is with the Electrical and Computer Engineering and Computer Science Departments, Purdue University, West Lafayette, USA (email: sbagchi@purdue.edu).

Biplab Banerjee is with the Centre of Studies in Resources Engineering (CSRE), Indian Institute of Technology Bombay, Mumbai, India (email: bbanerjee@iitb.ac.in).

Somali Chaterji is with the Agricultural and Biological Engineering Department, Purdue University, West Lafayette, USA (email: schaterji@purdue.edu).

target domain of embedded devices, a synchronous approach can get bottlenecked due to a few straggler clients as has been argued before [24], [18], [25]. This stems from the heterogeneity among the clients in resources and datasets, and variation in network connectivity [26]. Hence, in this work we choose to use an asynchronous federated learning optimization.

In this paper we discuss enabling action recognition in edge devices through federated learning. An overview of our approach is given in Figure 1. Considering that edge devices have limited computing and memory, the datasets present on them are small. To overcome this, we first distill knowledge from large models, pretrained on the larger Kinetics dataset, at the central server. We use two approaches to this knowledge distillation: one in which the teacher directly teaches the student [27], and the second approach, where there is an intermediate teaching assistant (TA) [28]. We observe that the latter approach is superior, albeit it comes at the cost of higher training time, and we adopt this approach in our pipeline. In the original work on TA, the setting was image classification. Here, we show through empirical evaluation that introducing a TA between the student and the teacher improves the accuracy for action recognition through videos. We further investigate the effects of using additional TAs in our pipeline. While the increase in per-clip, top-1 accuracy is appreciable when one TA is introduced, using additional TAs does not produce any considerable improvement in accuracy. On the other hand, the training time increases sharply as more TAs are added.

The advantage of knowledge distillation is twofold: first, it compresses the model—advantageous for limited computing, and second, it initializes a model for fine-tuning. Since we use heterogeneous embedded devices as clients, we incorporate an *asynchronous* federated optimization at the fine-tuning stage. We also show that under certain assumptions, the algorithm has a convergence bound. To the best of our knowledge, no previous work tackles the problem of performing action recognition from video clips, via federated learning. In addition to this, we compare our approach to two baselines: *first*, fine-tuning on the central server (no clients), and *second*, fine-tuning on clients using synchronous federated averaging. We use as evaluation metrics accuracy and time. For the accuracy, we use top-1 accuracy at the clip level¹, and at the entire video level. The finer granularity (clip-level) allows us to model (near) real-time action recognition and is a more challenging metric. For the metric of time, we measure both training and inference times.

In summary, our paper makes the following contributions:

1. Our work is the first to enable action recognition, a computationally heavy task, on edge devices, which have limited computing and memory resources and hence can only accommodate small-sized datasets on them.
2. In order to circumvent the problem of limited data, we apply knowledge distillation, with and without an intermediate teaching assistant (TA) using the Kinetics dataset, and observe that the latter is superior. Furthermore, we experiment by adding more TAs but observe that the increase in accuracy is negligible. Thus, our work expands on the original work to use TAs [28] to the significantly heavier task of activity recognition.

¹A clip consists of 8 video frames.

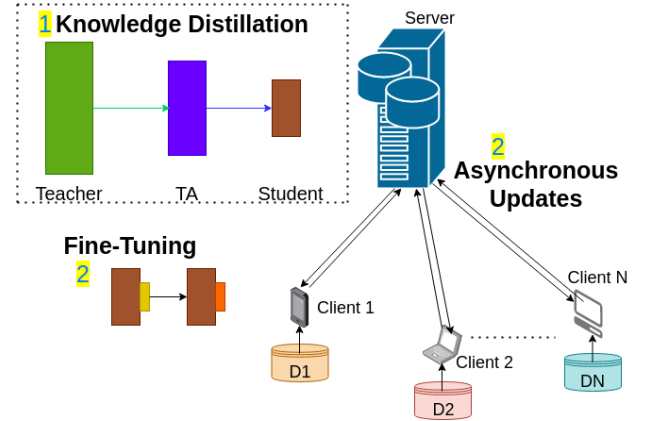


Fig. 1. The central server first performs knowledge distillation using the Kinetics dataset: from teacher to teaching assistant (TA) and from TA to student. The students (compressed models) are then fine-tuned on the smaller dataset using an asynchronous federated optimization.

3. The edge devices used as clients are heterogeneous, mimicking many real-world settings. We show a convergence bound for asynchronous training. We implement and run experiments on a heterogeneous testbed of embedded devices and show that the asynchronous training has significant advantages over synchronous, while the accuracy achieved is comparable to the centralized baseline.

II. RELATED WORK

FedVision [29] is the first paper to discuss setting up federated learning for object detection from images. Current approaches, which build object detection models on centrally located datasets, suffer from the high cost of transmitting video data and privacy concerns that are alleviated using federated learning. They provide a platform to support the development of object detection models. However, FedVision uses the synchronous FedAvg [30] algorithm in their work, which is adversely affected by stragglers and heterogeneity. Another approach [31], which tackles object detection, uses Kullback-Leibler divergence (KLD) to measure the divergence of the weight distribution in training and proposes FedAvg with Abnormal Weights Clip to relief the influence of non-IID data, enabling higher performance with non-IID data. Federated learning has also been used to solve problems in medical imaging [32]. To the best of our knowledge, no work so far has tackled the problem of action recognition using federated learning.

Federated distillation [33] follows an online version of knowledge distillation, known as co-distillation (CD) [34]. In CD, each device treats itself as a student, and sees the mean model output of all the other devices as its teacher's output. Furthermore, to rectify non-IID data of on-device ML can be corrected by obtaining the missing local data samples at each device from the other devices. This can induce significant overhead, so FAug is proposed which generates the missing data on each device. They empirically found that their approach yields lower overhead and better accuracy for image classification on MNIST [35]. Human action recognition

approaches can be categorized into visual sensor-based, non-visual sensor-based and multi-modal categories [2], [3]. So far, federated learning has only been incorporated into federated learning using wearable sensors [36], [37].

For federated learning on heterogeneous devices, previous work include an adaptive control algorithm that determines the best trade-off between local updates and global aggregation under a given resource constraint [38], model training in a network of heterogeneous edge devices, taking into account communication costs [39], and a method for straggler acceleration by dynamically masking neurons [40]. Aso-fed [41] presents an online learning algorithm that updates the central model in an asynchronous manner, tackling challenges associated with both varying computational loads at heterogeneous edge devices and stragglers. There has been a sparse but rapidly growing work in federated learning at edge devices, driven by the increasing numbers of such edge devices [42], [43], [38]. Training and deploying smaller yet accurate networks is of interest in edge devices. Knowledge distillation compresses the knowledge of a large and computationally expensive model (often an ensemble of neural networks) to a single computationally efficient neural network. The fact that these edge devices are often constrained in terms of local resources (compute, memory, and storage) as well as network resources (low bandwidth connections, intermittent connectivity) has given rise to fruitful areas of inquiry in communication-efficient federated learning [44], [45], [46], asynchronous learning to deal with stragglers [47], [40], approximate models and computation [48], [49], [50], and knowledge distillation to create more succinct models [51], [52].

When knowledge distillation is done via intermediate TAs, the accuracy for image classification is seen to increase [28]. Other applications of knowledge distillation in computer vision include those for semantic segmentation [53], [54], image classification [55], and action recognition [56]. To date, the applications of federated learning to computer vision have been limited. FedVision [29] provides a tool for the development of object detection frameworks. *Distinct from all prior work, we are the first to perform federated learning for action recognition, a computationally heavier task than those previously attempted, leveraging heterogeneous edge devices.*

III. BACKGROUND AND PROBLEM STATEMENT

A. Architecture

ResNets [57], [15] introduced shortcut connections that bypass a signal from one layer to the next. The connections pass through the gradient flows of networks from later layers to early layers, and ease the training of very deep networks. The ResNets that we use here performs 3D convolution and 3D pooling. Figure 2 shows the basic building block that we use while building our models. Here F refers to the number of convolution filters. The dimensions of $B(x)$ and x may be different, therefore, we use $1 \times 1 \times 1$ convolutions to match dimensions. In our experiments, we use ResNet-18, ResNet-26, and ResNet-34 which are derived from the building block. For the knowledge distillation experiments, the teacher we use is ResNet-34, the student is ResNet-18 and the teaching

assistant is ResNet-26. Subsequent fine-tuning is performed on the distilled ResNet-18 model.

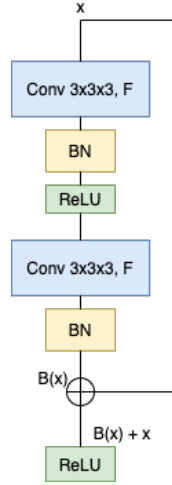


Fig. 2. ResNet building block

B. Knowledge Distillation

Knowledge distillation leverages information present in a larger “teacher” model to train a “smaller” student model. The soft probabilities (or logits) output from the teacher convey additional information to the student [27]: rather than just using training labels, students can learn more by understanding the relation between different classes. The additional information from the soft probabilities can help the student network identify the decision boundaries better if multiple classes have high soft probabilities.

Concretely, given an input \mathbf{x} , the teacher model computes a vector of scores (or logits) $\mathbf{z}^t(\mathbf{x}) = [z_1^t(\mathbf{x}), z_2^t(\mathbf{x}) \dots z_K^t(\mathbf{x})]$ for K classes. We define the knowledge distillation loss L_{KD} as the Mean Squared Error between the logits from the teacher model \mathbf{z}^t and the student model \mathbf{z}^s , *i.e.*, $L_{KD} = \|\mathbf{z}^t(x) - \mathbf{z}^s(x)\|^2$. The overall loss function is a combination of two loss functions, $L = \alpha L_{cls} + (1 - \alpha)L_{KD}$ where L_{cls} is the conventional cross-entropy loss which is computed for the predictions made by the student and the ground truth corresponding to the input \mathbf{x} .

The teacher model cannot effectively transfer its knowledge to the student if the size gap between them is large [28]. To alleviate this, the knowledge distillation is done in steps and an intermediate-sized model, the teaching assistant (TA), is introduced. Thus, in the first round of a *teacher-TA-student* knowledge distillation algorithm, the TA distills knowledge from the teacher model, with the loss function $L_1 = \alpha L_{cls}^{TA} + (1 - \alpha)L_{KD}^{TA}$. Subsequently, the student distills the knowledge that is gained by the TA and is trained with the loss function $L_2 = \alpha L_{cls}^S + (1 - \alpha)L_{KD}^S$. Here \mathbf{z}^{TA} refers to the vector of logits computed by the TA, $L_{KD}^{TA} = \|\mathbf{z}^t(x) - \mathbf{z}^{ta}(x)\|^2$, $L_{KD}^S = \|\mathbf{z}^{ta}(x) - \mathbf{z}^s(x)\|^2$, and L_{cls}^{TA} and L_{cls}^S are the cross-entropy losses for the TA and student model respectively, and these are calculated considering the ground truth to be the output of the teacher for the input \mathbf{x} .

C. Fine Tuning

Transfer learning is used to improve a learner from one domain by transferring information from a related domain. One possible need for transfer learning occurs when there is a limited supply of target training data [58]. Action recognition models require large datasets to learn complex spatiotemporal features [16]. In this work, we aim to enable edge devices with limited memory and computation abilities to perform action recognition. For example, amongst the edge devices we are using in this experiments, the NVIDIA Jetson AGX Xavier, the most well-resourced device type, has a 32GB storage and cannot store large datasets like Kinetics-400 which requires an approximate storage space of 400GB.

Next, we formally define transfer learning. A domain Ψ is defined by a feature space χ and a marginal probability distribution $P(X)$, where $X = \{\mathbf{x}_1, \mathbf{x}_2, \dots, \mathbf{x}_n\} \in \chi$. For a given domain Ψ , a task Γ is defined by a label space Y and a predictive function $f(\cdot)$. The training data consists of the pairs $\{\mathbf{x}_i, y_i\}$ where $\mathbf{x}_i \in \chi$ and $y_i \in Y$. Hence, we define a domain $\Psi = \{\chi, P(X)\}$ and a task $\Gamma = \{Y, f(\cdot)\}$. We define the source task Γ_S , target task Γ_T , source predictive function $f_S(\cdot)$, target predictive function $f_T(\cdot)$, source domain Ψ_S and target domain Ψ_T . Formally, transfer learning is the process of improving the predictive function $f_T(\cdot)$ using the related information from Ψ_S and T_S , where $\Psi_S \neq \Psi_T$ or $\Gamma_S \neq \Gamma_T$.

D. Problem Formulation

We consider a federated learning setup with n devices. Our aim is to find the parameters w that solve $\min_w F(w)$. Here, $F(w) = \frac{1}{n} \sum_{k=1}^n \mathbb{E}[l(w; d^k)]$ where d^k is data sampled from local data D^k on the k -th device, and $l(\cdot; \cdot)$ is a user specified loss function.

The training takes E global epochs. In the t^{th} epoch, the central server receives an updated w_{new} from a client. The model parameters are then averaged $w_t = (1 - \beta_t)w_{t-1} + \beta_t w_{new}$, where $\beta \in (0, 1)$ is the mixing hyperparameter. Because of the presence of stragglers, we define “staleness” as $t - \tau$ where τ is the epoch on the local device, and adaptively calculate the β_t . On the i^{th} device, after receiving the global model w_t , the local optimization is $\min_w \mathbb{E}[l(w; d^k) + \frac{\theta}{2} \|w - w_t\|^2] = \min_w \mathbb{E}[g_{w_t}(w; d^k)]$. Here θ is the regularization hyperparameter. All norms used in the paper are L_2 -norms. The model trains for a number of local iterations, where that number $\in [H_{min}, H_{max}]$ with a learning rate η . We define the imbalance ratio $\lambda = \frac{H_{max}}{H_{min}}$. $w_{t,h}^i$ refers to the weights from epoch t on device i after h training iterations. The number of iterations is specified by the server to the clients and it can do this based on local knowledge (such as, the desire to avoid hotspot congestion at the server) or based on client knowledge (such as, the compute resources at each edge device).

IV. ALGORITHMIC AND SYSTEM DETAILS

A. Asynchronous Federated Optimization

The global server and the clients conduct training in an asynchronous manner; the client starts training and sends updates to the server as soon as it is done. Because the clients

Algorithm 1 Asynchronous Federated Learning

Server

Initialize w_0 .

for $t = 1$ **to** E **do**

 Receive (w_{new}, τ) from any client

$\beta_t \leftarrow \beta \times s(t - \tau)$, $s(\cdot)$ is a function of the staleness

$w_t \leftarrow (1 - \beta_t)w_{t-1} + \beta_t w_{new}$

end for

Client

for $k \in \{1, \dots, n\}$ in parallel **do**

 receive global model and time stamp (w_t, t)

$\tau \leftarrow t$, $w_{\tau,0}^k \leftarrow w_t$

 Define $g_{w_t}(w; d) = l(x; z) + \frac{\theta}{2} \|w - w_t\|^2$

for local iteration $h \in \{1, \dots, H_\tau^k\}$ **do**

 Sample $d_{\tau,h}^k$ from D^k

$w_{\tau,h}^k \leftarrow w_{\tau,h-1}^k - \eta \nabla g_{w_t}(w_{\tau,h-1}^k; d_{\tau,h}^k)$

end for

 Send $(w_{\tau, H_\tau^k}^k, \tau)$ to the server

end for

are heterogeneous, there is no synchronization between the various devices. The k^{th} client performs training with a learning rate η using data $d_{\tau,h}^k$, which is randomly sampled from its local dataset D^k . H_τ^k is the number of local iterations performed. E is the total number of global epochs.

Because of delays by clients in sending the updates due to various reasons like low battery, high latency, or low bandwidth, different clients have different values of staleness, $t - \tau$. Intuitively, a large staleness means that the global model is more accurate because it has been trained more. Hence, aggregating with stragglers results in errors being introduced. To mitigate this, we use a function $s(t - \tau)$, which adaptively changes the mixing parameter $\beta_t = \beta \times s(t - \tau)$ — the weight allocated to w_{new} in the aggregation. The general form of this function is that $s(t - \tau) = 1$ when $t = \tau$ and it monotonically decreases with increase in $(t - \tau)$.

B. Convergence Analysis

We make the following assumptions in our analysis. Assumptions 1 and 2 are standard; typical examples are l_2 regularized linear regression, logistic regression, and softmax classification.

Assumption 1 Assume that $F(\cdot)$ is L-smooth; $\forall v, w, F(v) \leq F(w) + \langle \nabla F(w), v - w \rangle + \frac{L}{2} \|v - w\|^2$.

Assumption 2 Assume that $F(\cdot)$ is μ -weakly convex; there exists a function $G(\cdot)$ which is convex, such that $\forall v, G(v) = F(v) + \frac{\mu}{2} \|v\|^2$.

Assumption 3 The staleness of stragglers $t - \tau$, where t represents the current global epoch and τ represents the local epoch, is bounded $t - \tau \leq K$.

Assumption 4 Assume that for a device k , the square norm of the gradients are bounded. $\|\nabla l(w; d^k)\|^2 \leq B_1^2$ and $\|\nabla g_{w_t}(w; d^k)\|^2 \leq B_2^2$.

Theorem Under assumptions 1 through 4, for any constant $\epsilon > 0$, and choosing θ large enough such that $\theta > \mu$ and $-(1 + 2\theta + \epsilon)B_2^2 + (\theta^2 - \frac{\theta}{2})\|w_{\tau, h-1} - w_\tau\|^2 \geq 0 \forall w_{\tau, h}, w_\tau$, and learning rate $\eta < \frac{1}{L}$. After E global updates, algorithm 1 converges to a critical point,

$$\begin{aligned} \min_{t=0}^{E-1} E \|\nabla F(w_t)\|^2 &\leq \frac{\mathbb{E}[F(w_0) - F(w_E)]}{\beta\eta\epsilon EH_{min}} + \mathcal{O}\left(\frac{\eta\lambda^3 H_{min}^2}{\epsilon}\right) \\ &+ \mathcal{O}\left(\frac{\beta K \lambda}{\epsilon}\right) + \mathcal{O}\left(\frac{\eta K^2 \lambda^2 H_{min}}{\epsilon}\right) \\ &+ \mathcal{O}\left(\frac{\beta^2 \eta K^2 \lambda^2 H_{min}}{\epsilon}\right) \end{aligned}$$

Here $F(w_t)$, the objective function, represents the training loss in epoch t . Intuitively, when we upper bound the square of L2-norm of the gradient, $\nabla F(\cdot)$ approaches zero, and since we use gradient steps to update weights, the algorithm converges.

Choosing the learning rate $\eta = \frac{1}{\sqrt{E}}$, and having the number of training epochs (E) approach infinity, the asymptotic upper bound becomes:

$$\lim_{E \rightarrow \infty} \min_{t=0}^{E-1} E \|\nabla F(w_t)\|^2 \leq \mathcal{O}\left(\frac{\beta K \lambda}{\epsilon}\right)$$

The above asymptotic upper bound can be made arbitrarily close to zero by increasing ϵ .

Brief Outline of Proof

Take θ large enough such that $-(1 + 2\theta + \epsilon)B_2^2 + (\theta^2 - \frac{\theta}{2})\|w_{\tau, h-1} - w_\tau\|^2 \geq 0$

We write $\nabla g_{w_\tau}(w_{\tau, h-1}^i, d_{\tau, h}^i)$ as $\nabla g_{w_\tau}(w_{\tau, h-1})$ for simplicity.

$$\begin{aligned} &\langle \nabla G_{w_\tau}(w_{\tau, h-1}), \nabla g_{w_\tau}(w_{\tau, h-1}) \rangle - \epsilon \|\nabla F(w_{\tau, h-1})\|^2 \\ &= \langle \nabla F(w_{\tau, h-1}) + \theta(w_{\tau, h-1} - w_\tau), \nabla l(w_{\tau, h-1}) + \theta(w_{\tau, h-1} - w_\tau) \rangle - \epsilon \|\nabla F(w_{\tau, h-1})\|^2 \\ &= \langle \nabla F(w_{\tau, h-1}), \nabla l(w_{\tau, h-1}) \rangle + \theta \langle \nabla F(w_{\tau, h-1}) + \nabla l(w_{\tau, h-1}), w_{\tau, h-1} - w_\tau \rangle + \theta^2 \|w_{\tau, h-1} - w_\tau\|^2 - \epsilon \|\nabla F(w_{\tau, h-1})\|^2 \\ &\geq -0.5 \|\nabla F(w_{\tau, h-1})\|^2 - 0.5 \|\nabla l(w_{\tau, h-1})\|^2 - 0.5\theta \|\nabla F(w_{\tau, h-1}) + \nabla l(w_{\tau, h-1})\|^2 - 0.5\theta \|w_{\tau, h-1} - w_\tau\|^2 + \theta^2 \|w_{\tau, h-1} - w_\tau\|^2 - \epsilon \|\nabla F(w_{\tau, h-1})\|^2 \\ &\geq -0.5 \|\nabla F(w_{\tau, h-1})\|^2 - 0.5 \|\nabla l(w_{\tau, h-1})\|^2 - \theta \|\nabla F(w_{\tau, h-1})\|^2 - \theta \|\nabla l(w_{\tau, h-1})\|^2 - 0.5\theta \|w_{\tau, h-1} - w_\tau\|^2 + \theta^2 \|w_{\tau, h-1} - w_\tau\|^2 - \epsilon \|\nabla F(w_{\tau, h-1})\|^2 \geq -(1 + 2\theta + \epsilon)B_2^2 + (\theta^2 - \frac{\theta}{2})\|w_{\tau, h-1} - w_\tau\|^2 \geq 0 \end{aligned}$$

$$\implies \eta \langle \nabla G_{w_\tau}(w_{\tau, h-1}), \nabla g_{w_\tau}(w_{\tau, h-1}) \rangle \leq \eta \epsilon \|\nabla F(w_{\tau, h-1})\|^2 \quad (1)$$

Using $\tau - (t - 1) \leq K$, we have $\|w_\tau - w_{t-1}\|^2 \leq \|(w_\tau - w_{\tau-1}) + \dots + (w_{t-1} - w_{t-1})\|^2$

$$\leq K \|(w_\tau - w_{\tau-1})\|^2 + \dots + K \|(w_{t-1} - w_{t-1})\|^2 \leq \beta^2 \eta^2 K^2 \lambda^2 H_{min}^2 \mathcal{O}(B_2^2)$$

$$\|w_\tau - w_{t-1}\|^2 \leq \beta^2 \eta^2 K^2 \lambda^2 H_{min}^2 \mathcal{O}(B_2^2) \quad (2)$$

Also, $\|w_\tau - w_{t-1}\| \leq \|(w_\tau - w_{\tau-1}) + \dots + (w_{t-1} - w_{t-1})\| \leq \|w_\tau - w_{\tau-1}\| + \dots + \|w_{t-1} - w_{t-1}\| \leq \beta \eta K \lambda H_{min} \mathcal{O}(B_\epsilon)$

$$\|w_\tau - w_{t-1}\| \leq \beta \eta K \lambda H_{min} \mathcal{O}(B_2) \quad (3)$$

Consider L-smoothness and convexity assumptions,

$$\begin{aligned} \mathbb{E}[F(w_{\tau, h}) - F(w_*)] &\leq \mathbb{E}[G_{w_\tau}(w_{\tau, h}) - F(w_*)] \\ &\leq G_{w_\tau}(w_{\tau, h}) - F(w_*) - \eta \mathbb{E}[\langle \nabla G_{w_\tau}(w_{\tau, h-1}), \nabla g_{w_\tau}(w_{\tau, h-1}) \rangle] + 0.5L\eta^2 \mathbb{E}[\|\nabla g_{w_\tau}(w_{\tau, h-1})\|^2] \\ &\leq F(w_{\tau, h}) - F(w_*) + 0.5\theta \|w_{\tau, h-1} - w_\tau\|^2 - \eta \mathbb{E}[\langle \nabla G_{w_\tau}(w_{\tau, h-1}), \nabla g_{w_\tau}(w_{\tau, h-1}) \rangle] + 0.5L\eta^2 \mathbb{E}[\|\nabla g_{w_\tau}(w_{\tau, h-1})\|^2] \\ &\leq F(w_{\tau, h}) - F(w_*) - \eta \mathbb{E}[\langle \nabla G_{w_\tau}(w_{\tau, h-1}), \nabla g_{w_\tau}(w_{\tau, h-1}) \rangle] + 0.5L\eta^2 B_2^2 + \frac{\theta}{2} \eta^2 \lambda^2 H_{min}^2 B_2^2 \\ &\leq F(w_{\tau, h}) - F(w_*) - \eta \mathbb{E}[\langle \nabla G_{w_\tau}(w_{\tau, h-1}), \nabla g_{w_\tau}(w_{\tau, h-1}) \rangle] + \eta^2 \mathcal{O}(\theta \lambda^2 H_{min}^2 B_2^2) \\ &\leq F(w_{\tau, h}) - F(w_*) - \eta \epsilon \|\nabla F(w_{\tau, h-1})\|^2 + \eta^2 \mathcal{O}(\theta \lambda^2 H_{min}^2 B_2^2) \text{ (Using 1)} \end{aligned}$$

Rearrange and telescope,

$$\mathbb{E}[F(w_{\tau, h}) - F(w_\tau)] \leq -\eta \epsilon \sum_{h=0}^{H-1} \mathbb{E} \|\nabla F(w_{\tau, h})\|^2 + \eta^2 \mathcal{O}(\theta \lambda^3 H_{min}^3 B_2^2) \quad (4)$$

Using L-smoothness,

$$\begin{aligned}
F(w_\tau) - F(w_{t-1}) &\leq \langle \nabla F(w_{t-1}), w_\tau - w_{t-1} \rangle + \frac{L}{2} \|w_\tau - w_{t-1}\|^2 \\
&\leq \|\nabla F(w_{t-1})\| \|w_\tau - w_{t-1}\| + \frac{L}{2} \|w_\tau - w_{t-1}\|^2 \\
&\leq B_1 \beta \eta K \lambda H_{min} \mathcal{O}(B_2) + \frac{L}{2} \beta^2 \eta^2 K^2 \lambda^2 H_{min}^2 \mathcal{O}(B_2^2) \text{ (Using 2 and 3)} \\
&\leq B_1 \beta \eta K \lambda H_{min} \mathcal{O}(B_2) + \beta^2 \eta^2 K^2 \lambda^2 H_{min}^2 \mathcal{O}(B_2^2)
\end{aligned}$$

$$F(w_\tau) - F(w_{t-1}) \leq \beta \eta K \lambda H_{min} \mathcal{O}(B_1 B_2) + \beta^2 \eta^2 K^2 \lambda^2 H_{min}^2 \mathcal{O}(B_2^2) \quad (5)$$

Consider,

$$\begin{aligned}
\mathbb{E}[F(w_t) - F(w_{t-1})] &\leq \mathbb{E}[G_{w_{t-1}}(w_t) - F(w_{t-1})] \\
&\leq \mathbb{E}[(1 - \beta)G_{w_{t-1}}(w_{t-1}) + \beta G_{w_{t-1}}(w_{\tau,h}) - F(w_{t-1})] \\
&\leq \mathbb{E}[\beta(F(w_{\tau,h}) - F(w_{t-1})) + \frac{\beta\theta}{2} \|w_{\tau,h} - w_{t-1}\|^2] \leq \beta \mathbb{E}[F(w_{\tau,h}) - F(w_{t-1})] + \beta\theta \|w_{\tau,h} - w_\tau\|^2 + \beta\theta \|w_\tau - w_{t-1}\|^2 \\
&\leq \beta \mathbb{E}[F(w_{\tau,h}) - F(w_{t-1})] + \beta\theta \beta^2 \eta^2 K^2 \lambda^2 H_{min}^2 \mathcal{O}(B_2^2) \text{ (Using 2)}
\end{aligned}$$

Using 4 and 5,

$$\begin{aligned}
\mathbb{E}[F(w_t) - F(w_{t-1})] &\leq -\beta \eta \epsilon \sum_{h=0}^{H-1} \mathbb{E} \|\nabla F(w_{\tau,h})\|^2 + \eta^2 \mathcal{O}(\theta \lambda^3 H_{min}^3 B_2^2) + \beta^2 \eta K \lambda H_{min} \mathcal{O}(B_1 B_2) + \beta^3 \eta^2 K^2 \lambda^2 H_{min}^2 \mathcal{O}(B_2^2) + \\
&\beta \eta^2 K^2 \lambda^2 H_{min}^2 \mathcal{O}(B_2^2)
\end{aligned}$$

Note that H_t is the number of local epochs applied in iteration t . Rearrange terms to get,

$$\sum_{h=0}^{H_t-1} \mathbb{E} \|\nabla F(w_{\tau,h})\|^2 \leq \frac{\mathbb{E}[F(w_t) - F(w_{t-1})]}{\beta \eta \epsilon} + \frac{\eta \lambda^3 H_{min}^3 \mathcal{O}(B_2^2)}{\epsilon} + \frac{\beta K \lambda H_{min} \mathcal{O}(B_1 B_2)}{\epsilon} + \frac{\beta^2 \eta K^2 \lambda^2 H_{min}^2 \mathcal{O}(B_2^2)}{\epsilon} + \frac{\eta K^2 \lambda^2 H_{min}^2 \mathcal{O}(B_2^2)}{\epsilon}$$

By Telescoping and taking total expectation, after T global epochs, we have

$$\begin{aligned}
\min_{t=0}^{E-1} \mathbb{E} \|\nabla F(w_t)\|^2 &\leq \frac{1}{\sum_{t=1}^T H_t} \sum_{t=1}^T \sum_{h=0}^{H_t-1} \mathbb{E} \|\nabla F(w_{\tau,h})\|^2 \\
&\leq \frac{\mathbb{E}[F(w_0) - F(w_E)]}{\beta \eta \epsilon E H_{min}} + \mathcal{O}\left(\frac{\eta \lambda^3 H_{min}^3}{\epsilon}\right) + \mathcal{O}\left(\frac{\beta K \lambda}{\epsilon}\right) + \mathcal{O}\left(\frac{\eta K^2 \lambda^2 H_{min}}{\epsilon}\right) + \mathcal{O}\left(\frac{\beta^2 \eta K^2 \lambda^2 H_{min}}{\epsilon}\right)
\end{aligned}$$

This concludes the proof for the convergence bound of the asynchronous federated algorithm. In the experimental evaluation, we tune hyperparameters, such as β in Figure 10 and observe how the convergence varies.

V. EXPERIMENTAL EVALUATION

The central server in the following experiments has an NVIDIA Tesla V100S 32GB GPU. We use a variety of clients to demonstrate that our asynchronous federated optimization is robust to heterogeneous edge devices: *NVIDIA Jetson Nano*, which has 4GB memory, and a 128-core Maxwell GPU; *NVIDIA Jetson TX2*, which has 8GB memory, and a 256-core Pascal GPU; *NVIDIA Jetson Xavier NX*, which has a 8GB memory, and a 384-core Volta GPU with 48 Tensor cores; and *NVIDIA Jetson AGX Xavier*, which has 32GB memory and 512-core Volta GPU. The Kinetics [12] dataset, which we use for knowledge distillation, is present at the central server, and we conduct experiments on two datasets for fine-tuning: HMDB51 [13] and UCF101 [14]. This data is distributed amongst the clients. The Kinetics dataset contains 400 human action classes, with at least 400 video clips for each action. Each clip lasts for around 10s and is taken from a different YouTube video. The dataset has 306,245 videos, and is divided into three splits: one for training, having 250–1000 videos per class; one for validation, with 50 videos per class; and one for testing, with 100 videos per class. The HMDB51 dataset contains 51 classes and a total of 3,312 videos. The UCF101 dataset consists of 101 classes and over 13k clips (27 hours of video data).

In this paper, we use two metrics for evaluation of our pipeline: per-clip and per-video accuracy. Similar to a previous study [16], we use the **per-clip top-1** accuracy as an evaluation metric, *i.e.*, if we consider a 10 second video at 24 fps and 8 frames per clip are used, we get 30 clips. The top-1 refers to considering the model prediction to be accurate if the top class it outputs matches the label of the video. Most previous studies report the per-video accuracy by taking the mean of class scores output from all clips in a video and comparing it to the ground truth. We choose one of the evaluation metrics to be per-clip granularity level because it indicates how noisy the videos in a dataset are and it opens up scope for future work in which predictions can be made on clips rather than using the entire video — the per-clip evaluation also allows for real-time predictions. We also use the **per-video top-1** accuracy, in which we take the mean of class scores output from all clips in a video and compare it to the ground truth

A. Knowledge Distillation

In the first stage of our pipeline, we perform knowledge distillation from a larger model, trained on the Kinetics dataset. We compare three approaches in order to validate using knowledge distillation with an intermediate TA. For these experiments, we use a batch size of 128, learning rate $\eta = 0.1$, and an SGD optimizer with a weight decay 0.001 and momentum 0.9. In the first experiment, we train a ResNet-18 model from scratch on the Kinetics dataset and the per-clip top-1 accuracy achieved is 50.2%. Using knowledge distillation, the accuracy is improved to 53.8% when we distill directly from ResNet-34 to ResNet-18, and 54.6% when we use a ResNet-26 as the intermediate TA between the teacher and student. From Figure 3, it is evident that using a distilled ResNet-18 is better than using a ResNet-18 trained from scratch. There is a

counter pull from the training time — the KD approach (not counting the time to train the ResNet-34) takes 43% longer than training from scratch (the ResNet-18). This can be explained by the fact that “Train from scratch” includes only forward-backward passes on ResNet-18 with optimization using only cross-entropy loss. On the other hand, KD involves forward passes on the larger ResNet-34, forward-backward passes on ResNet-18, and optimization on ResNet-18 using a combination of both cross-entropy loss and the MSE on the logits (recall that we are fine-tuning only the last FC layer). This timing result is consistent with prior works that report on the timing performance of knowledge distillation [27], [59].

We further investigate using multiple TAs. From Table II, we see that the introduction of one TA increases the train time from 44 hours 58 minutes to 55 hours 23 minutes and the corresponding increase in per-clip accuracy is 0.8%. Hence, there is a trade-off between increased training time and increased accuracy. Furthermore, the introduction of a TA almost always increases accuracy but the optimal number of TAs and size of each is an open research question [28]. Additionally, TAs are used to bridge the gap between the student and teacher: by using a ResNet-26 between ResNet-34 and ResNet-18 we already accomplish this. If the gap between the teacher and student were larger, using additional TAs would be of benefit at the expense of increased computation and train time required. In order to reduce the train times and achieve comparable accuracy to the baselines, we use one TA.

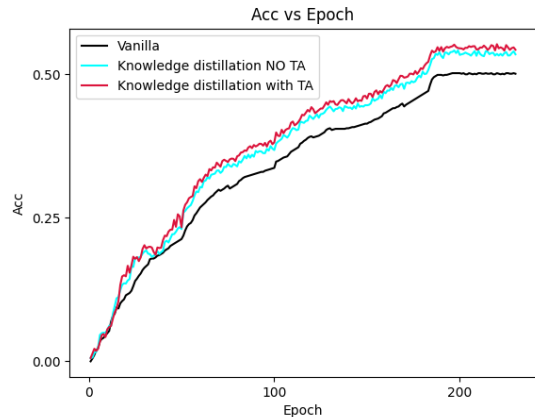


Fig. 3. Top-1 accuracy on the Kinetics validation dataset for 3 experiments: 1. Training a ResNet-18 from scratch (Vanilla); 2. Knowledge distillation from ResNet-34 to ResNet-18 (Knowledge Distillation with no TA); 3. Knowledge distillation with ResNet-34 Teacher, ResNet-26 TA, and ResNet-18 Student (Knowledge Distillation with TA).

We further investigate the effects of using additional TAs in our pipeline. In all these experiments, distillation is performed from teacher ResNet-34 to student ResNet-18. In the first experiment, we do not use any TAs. In the next experiment, we use ResNet-26 as a TA. The third experiment is performed using two TAs: ResNet-28 and ResNet-24, and in the final experiment, we use three TAs: ResNet-30, ResNet-26, and ResNet-22. The architectures have been outlined in Figure 4. From Table I, we see that while the increase in **per-clip top-1** accuracy is appreciable when one TA is introduced, using additional TAs does not produce any considerable improvement

TABLE I

KNOWLEDGE DISTILLATION IS PERFORMED BY VARYING THE NUMBER OF INTERMEDIATE TEACHING ASSISTANTS (TAS).

# TAS	EPOCHS	TIME (HRS, MINS) (INCREASE)	PER-CLIP ACCURACY
0	200	44 H 58 M (0%)	53.8%
1	200	55 H 23 M (23.2%)	54.6%
2	200	69 H 35 M (54.7%)	54.8%
3	200	85 H 47 M (90.8%)	54.9%

in accuracy. The training time increases sharply as more TAS are added. Hence, in the subsequent stages in our pipeline, we chose to use a single TA.

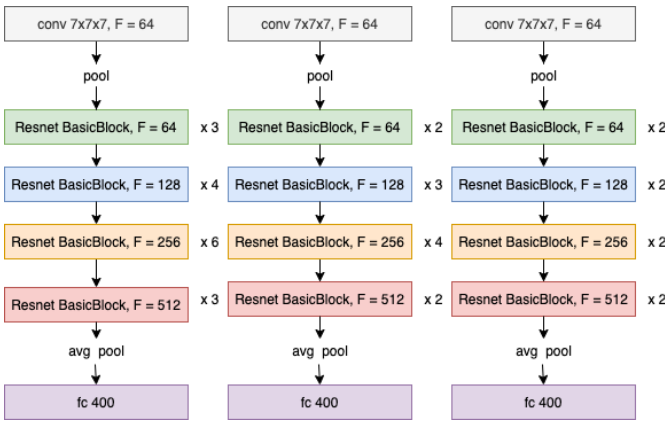


Fig. 4. ResNet-34, ResNet-26, and ResNet-18 architectures derived from the basic building block

For the rest of the experiments, we perform fine-tuning, by reinitializing the fully connected layer — the last layer in the ResNet-18 model. The ResNet-18 being used is the model distilled from ResNet-34 (trained on the Kinetics dataset) via a ResNet-26 TA. The first baseline experiment that we perform is fine-tuning on the central server when no clients are present; the per-clip top-1 accuracy is shown in Figure 5 for HMDB51 and Figure 6 for UCF101. A model trained in this manner achieves a per-clip top-1 accuracy of 57.3% on HMDB51. In contrast, ResNet-18 trained from scratch on HMDB51 achieves a per-clip accuracy of only 17.1%. This is consistent with several prior results that have indicated the difficulty of achieving high accuracy in activity recognition on the relatively small HMDB51 dataset [16], [60].

B. Transfer Learning

The Kinetics-400 dataset requires an approximate disk space of 400GB to store. Amongst the edge devices we are using in these experiments, the most well-endowed, NVIDIA Jetson AGX Xavier has only 32GB storage. Hence, edge devices can only accommodate smaller-sized datasets on them². In this section, we use the HMDB51 dataset and the UCF101 for evaluation. The HMDB51 which has a size of 2,062MB and

²One may argue that adding cheap external storage such as through Flash cards can alleviate this problem. However, reading from external storage is orders of magnitude slower than reading from internal storage and will thus increase the training time to an infeasible level.

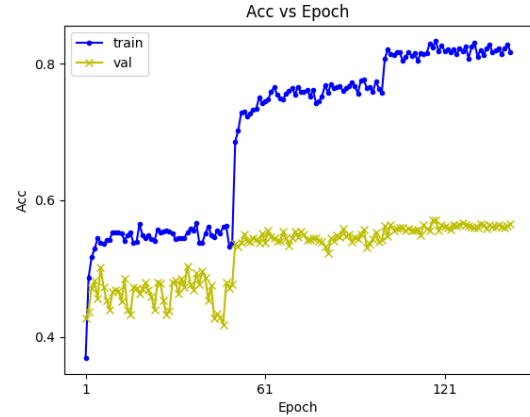


Fig. 5. ResNet-18, distilled from ResNet-34, via a ResNet-26 Teaching assistant, and fine-tuned on HMDB51. The fine-tuning is performed at the central server without any clients.

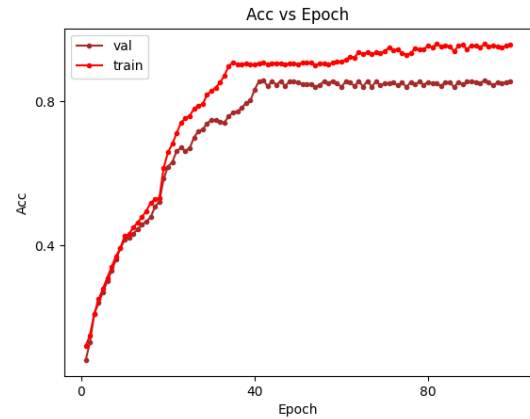


Fig. 6. ResNet-18, distilled from ResNet-34, via a ResNet-26 Teaching assistant, and fine-tuned on UCF101, performed at the central server without any clients.

is distributed amongst the clients in such a way that requires approximately 500MB of storage space on each client. The UCF101 is 6.9GB and each client has about 1.725GB of data. Once we have distilled knowledge from the larger ResNet-34, trained on the Kinetics dataset to the ResNet-18 architecture via a TA, the next step is to fine-tune on the smaller dataset; *i.e.*, HMDB51 or UCF101.

In the transfer learning experiments, we fine-tune only the last fully connected layer. We observed that the accuracy reduces as we increase the number layers that we fine-tune. In baseline experiments, we use a synchronous federated optimization, with 4 clients, one of each type (recall there are 4 kinds of embedded devices in our testbed). The accuracy vs. number of global aggregations (epochs) is shown in Figure 7 for HMDB51, and Figure 8 for UCF101. For each aggregation that the central server performs, the number of local epochs is 3. We use a batch size of 8, learning rate $\eta = 0.001$, SGD optimizer with momentum 0.9. Each clip has 8 frames, which are taken from the corresponding video. Although increasing the number of frames per clip would have increased the accuracy, doing so causes the clients to throw a CUDA out of memory error.

From Table II, refer to the HMDB51 experiments. We

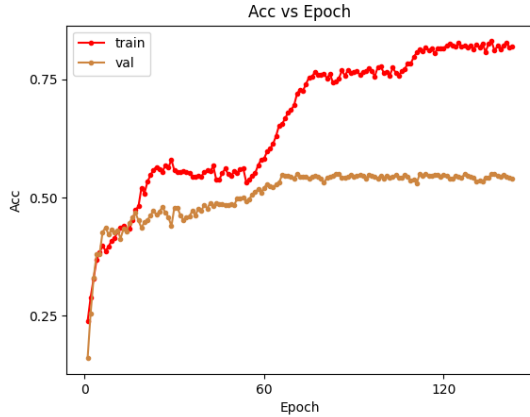


Fig. 7. Fine-tuning on HMDB51 using a synchronous FedAvg algorithm. The clients connected to the central server are heterogeneous in their computational resources. For comparison, ResNet-18 trained from scratch on HMDB51 achieves a per-clip accuracy of 17.1%.

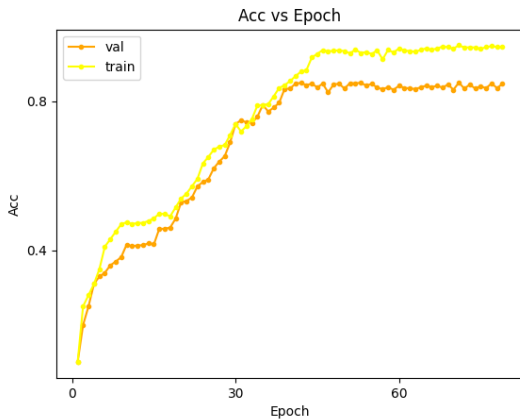


Fig. 8. Fine-tuning on UCF101 using a synchronous FedAvg algorithm. The accuracy shown is the per-clip video accuracy.

see that the time required for a synchronous optimization is 10 hours and 54 minutes. In contrast, the asynchronous federated algorithm takes only 6 hours and 31 minutes, a 40% decrease. This can be attributed to the clients having different computing resources, and hence requiring different amounts of time to complete the local epochs as given in Table IV. While the synchronous algorithm has to wait for the slowest client to send its update, the asynchronous algorithm continues its optimization. A similar effect is observed in the case of UCF101. One may wonder that it is beneficial to use the approach of fine tuning at the server without any clients (for HMDB51 and UCF101) and thus not having to use our approach. This alternate method runs into the problem that it does not leverage federated learning, which has its traditional benefits of scaling to a large number of clients (and thus not needing heavyweight server) and preserving privacy of client data. The same argument applies to why we would not want to train for the Kinetics data from scratch (this would obviously have to be done at the server).

As can be seen in Table III, the asynchronous training achieves higher accuracy for both per-clip and per-video metrics. This emphasizes the importance of our design of dealing

TABLE II

THE TIME REQUIRED FOR VARIOUS STAGES SHOWN IN FIGURE 1 AND THE BASELINE EXPERIMENTS. KD REFERS TO KNOWLEDGE DISTILLATION, SYNCHRONOUS REFERS TO FINE-TUNING USING FEDAVG, ASYNCHRONOUS REFERS TO FINE-TUNING USING ASYNCHRONOUS FEDERATED OPTIMIZATION. THE FINE-TUNING IS PERFORMED USING RESNET-18, DISTILLED FROM RESNET-34 VIA A RESNET-26 TEACHING ASSISTANT.

DATASET	TASK	EPOCHS	TIME
KINETICS	TRAIN FROM SCRATCH	200	31 HRS 26 MINS
KINETICS	KD (NO TA)	200	44 HRS 58 MINS
KINETICS	KD (TA)	200	55 HRS 23 MINS
HMDB51	FINE-TUNE NO CLIENTS	80	3HRS 15MINS
HMDB51	SYNCHRONOUS	80	10 HRS 54 MINS
HMDB51	ASYNCHRONOUS	80	6 HRS 31 MINS
UCF101	FINE-TUNE NO CLIENTS	80	22 HRS 5 MINS
UCF101	SYNCHRONOUS	80	74 HRS 27 MINS
UCF101	ASYNCHRONOUS	80	44 HRS 7 MINS

with different rates of progress of different clients in the asynchronous training approach. From Table III we also see that our model performs better on UCF101 compared to HMDB51. HMDB51 contains several categories about different facial movements like smiling, laughing, chewing, and several other categories like eating and drinking. Such categories are not present in the list of categories of the data set UCF101 and are among the most difficult categories to deal with. Current state-of-the-art for UCF101 and HMDB51 stand at per-video top-1 accuracy of 98.69% and 85.10% respectively and are produced by the same work [61]. Hence, it is evident that the HMDB51 is a difficult dataset to classify for deep learning architectures.

TABLE III

THE TOP-1 PER-CLIP ACCURACY AND THE TOP-1 PER-VIDEO ACCURACY

DATASET	TASK	PER-CLIP	PER-VIDEO
HMDB51	FINE-TUNE NO CLIENTS	57.3%	64.1%
HMDB51	SYNCHRONOUS	54.4%	61.8%
HMDB51	ASYNCHRONOUS	55.6%	62.3%
UCF101	FINE-TUNE NO CLIENTS	85.7%	91.1%
UCF101	SYNCHRONOUS	84.3%	89.3%
UCF101	ASYNCHRONOUS	84.4%	89.5%

C. Asynchronous Learning Hyperparameters

The asynchronous algorithm that we use adaptively updates the global model using the mixing hyperparameter β and the function $s(t - \tau) = (1 + t - \tau)^{-a}$. The function $s(\cdot)$ is monotonically decreasing with the staleness $t - \tau$. The intuition behind this is that in the time required for one client to perform local training and send its updates to the central server, several aggregations may have been performed at the central server. Hence, the global model has already learned more compared to the outdated updates that the client sends in. We perform experiments in order to find the best combination of the hyperparameters a and β . In Figure 9, we keep $\beta = 0.7$ and vary a , here $a = 0$ refers to the case when we do not adjust the mixing parameter to account for stragglers: $\beta_t = \beta$. We see

that $a = 0.5$ is the best choice; not only is the convergence the fastest, the per-clip top-1 accuracy achieved for HMDB51 is the highest 55.6% — $a = 0$ gives an accuracy of 53.9%, $a = 0.3$ gives 54.2% and $a = 0.9$ gives 53.7%. Therefore, we conclude that it’s good to penalize clients for being late; however, keeping large penalties, such as $a = 0.9$, will adversely affect speed of convergence since the weight assigned to updates received from clients will be very small during aggregation. Figure 11 shows the corresponding experiment for UCF101. We again observe that keeping $a = 0.5$ gives the best results — $a = 0$ and $a = 0.3$ give a per-clip accuracy of 83.7%, $a = 0.5$ gives 84.4% and $a = 0.9$ gives 83.6%.

TABLE IV

RESNET-18 TRAIN TIMES PER EPOCH. FOR HMDB51 AND UCF101, EACH CLIENT HAS APPROXIMATELY 500MB AND 1.73GB OF VIDEO DATA RESPECTIVELY.

DATASET	DEVICE	TRAIN TIME (PER LOCAL EPOCH)
HMDB51	NVIDIA JETSON NANO	391.1 SECONDS
HMDB51	NVIDIA JETSON TX2	293.1 SECONDS
HMDB51	NVIDIA JETSON XAVIER NX	121.3 SECONDS
HMDB51	NVIDIA JETSON AGX XAVIER	84.5 SECONDS
UCF101	NVIDIA JETSON NANO	2691.6 SECONDS
UCF101	NVIDIA JETSON TX2	2001.4 SECONDS
UCF101	NVIDIA JETSON XAVIER NX	821.9 SECONDS
UCF101	NVIDIA JETSON AGX XAVIER	572.1 SECONDS

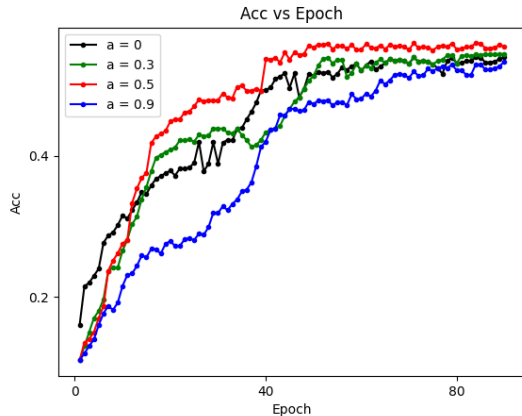


Fig. 9. The function $s(t - \tau) = (1 + t - \tau)^{-a}$ takes as an input the “staleness” $t - \tau$. We set the mixing hyperparameter $\beta = 0.7$ and vary the hyperparameter a . The asynchronous federated aggregation at the central server is adaptive; $\beta_t = \beta \times s(t - \tau)$ and $w_t = (1 - \beta_t)w_{t-1} + \beta_t w_{new}$. The figure depicts Asynchronous federated optimization performed on HMDB51.

In the next set of experiments, we set $a = 0.5$ and vary β . For HMDB51, $\beta = 0.7$ gives the best per-clip accuracy of 55.6%. Keeping a very low value assigns lower weight to the updates from the client during aggregation, and as can be seen in Figure 10 the model’s convergence slows down and leads to lower accuracy upon convergence — $\beta = 0.3$ gives 53.6%, $\beta = 0.5$ gives 53.8%. A high value of the mixing parameter $\beta = 0.9$ gives 51.4%. The low accuracy can be attributed to the fact that the dataset is distributed amongst many clients so assigning too high a weight to any client will lead to the model becoming biased. For the experiments on UCF101 as seen in Figure 12, setting $a = 0.5$, $\beta = 0.7$ gives the best per-clip accuracy — $\beta = 0.3$ gives 83.2%, $\beta = 0.5$ gives 83.5%, $\beta = 0.7$ gives 84.4% and $\beta = 0.9$ gives 82.3%.

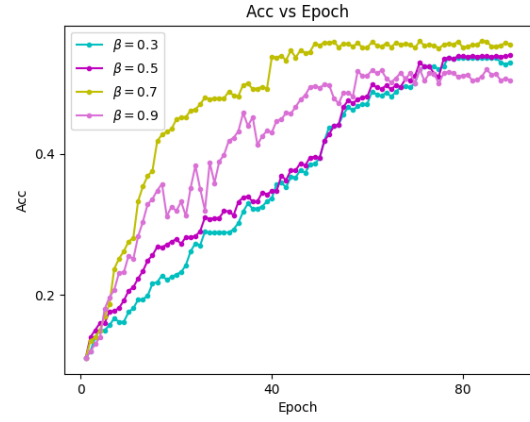


Fig. 10. We set $a = 0.5$ & vary the mixing hyperparameter β . In the asynchronous federated optimization, convergence for small β is slow as this corresponds to a smaller weight being assigned to the updated parameters received from the clients during aggregation. The figure depicts Asynchronous federated optimization performed on HMDB51.

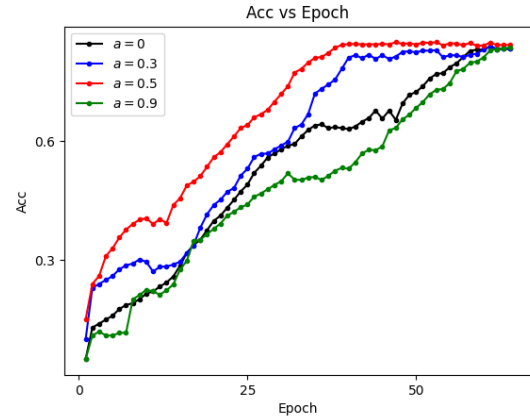


Fig. 11. Asynchronous federated optimization performed on UCF101. We set the mixing hyperparameter $\beta = 0.7$ and vary the hyperparameter a .

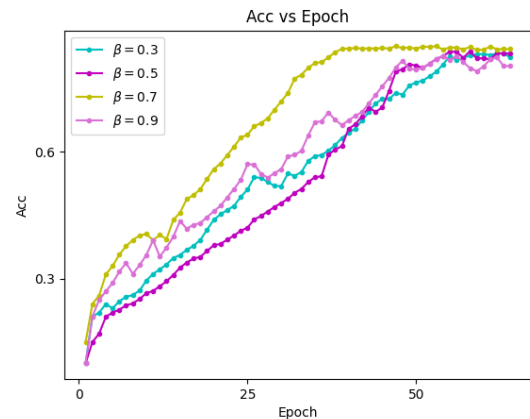


Fig. 12. Asynchronous federated optimization performed on UCF101. We set $a = 0.5$ & vary the mixing hyperparameter β .

The combination of hyperparameters $a = 0.5$ and $\beta = 0.7$ gives the best results for both UCF101 and HMDB51. The **top-1 per-video** setting $a = 0.5$ and $\beta = 0.7$ is 62.3% and 89.5% respectively. Table V shows the inference times on the

entire test dataset for the ResNet-18 architecture. From this and Table IV, it is clear that each client requires different amounts of time to train. For example, from Table IV we see that the training time per epoch is 4.7X more expensive on the Jetson Nano (the lowest spec of the four kinds of embedded devices) compared to the AGX Xavier (the highest spec). Therefore, this emphasizes the need for an asynchronous federated learning strategy rather than a synchronous one when dealing with heterogeneous embedded devices.

TABLE V
RESNET-18 EVALUATED ON THE ENTIRE TEST DATASET. THE DEVICE HETEROGENEITY IS REFLECTED IN THE INFERENCE TIMES.

DATASET	DEVICE	TEST TIME
HMDB51	NVIDIA JETSON NANO	181.4 SECONDS
HMDB51	NVIDIA JETSON TX2	116.3 SECONDS
HMDB51	NVIDIA JETSON XAVIER NX	89.4 SECONDS
HMDB51	NVIDIA JETSON AGX XAVIER	68.3 SECONDS
UCF101	NVIDIA JETSON NANO	621.3 SECONDS
UCF101	NVIDIA JETSON TX2	381.2 SECONDS
UCF101	NVIDIA JETSON XAVIER NX	322.5 SECONDS
UCF101	NVIDIA JETSON AGX XAVIER	217.7 SECONDS

VI. DISCUSSION

Our aim is to enable edge devices to perform action recognition, a computationally heavy task. Since in the real world, there is a mix of heterogeneous devices at the edge, we set out to develop our solution for such heterogeneity. Action recognition models have large datasets needed to learn complex spatio-temporal features—Kinetics-400 is approximately 400GB in size—and edge devices do not have this much disk space available. The largest from amongst our clients, NVIDIA Jetson AGX Xavier, has 32GB of storage. Datasets present on the edge devices, such as the HMDB51 (2GB), result in the ResNet-18 model overfitting (per-clip, top-1 accuracy of only 17.1%). The solution to this is transfer learning: pre-training on the Kinetics dataset and fine-tuning on smaller datasets such as HMDB51 and UCF101. Our experiments on Kinetics show that a ResNet-18, trained from scratch, achieves a per-clip top-1 accuracy of 50.2%, ResNet-18 distilled directly from ResNet-34 gives an accuracy of 53.8%, and ResNet-18 distilled from a trained ResNet-34 via a teaching assistant (TA) achieves an accuracy of 54.6%. Consequently, we use the ResNet-18 model distilled via a TA for fine-tuning. Furthermore, our experiments show that using the increment in accuracy from no TA to one TA is appreciable, however; adding more TAs results in negligible change in accuracy but increases the training time. Next, we experiment with federated optimization for a heterogeneous set of client devices. Heterogeneous devices pose a challenge for synchronous optimization: such aggregation will happen only after all devices send their updates. We therefore propose to use asynchronous federated averaging for our target scenario of heterogeneous embedded devices. We start off by analytically proving the convergence bound for our asynchronous approach. We empirically see that our asynchronous federated training takes 40% less time than its synchronous counterpart. We also

perform hyperparameter tuning of the asynchronous algorithm and determine that $\alpha = 0.5$ and $\beta = 0.7$ gives the best accuracy for both HMDB51 and UCF101, which is not far behind the central server fine-tuning with no clients—for HMDB51, the per-clip accuracy for the federated asynchronous optimization is 55.6%, as compared to 57.3% on the central server with no clients. Thus, we for the first time empirically show that it is possible to achieve activity recognition on edge devices that are available available today.

In future work, one may consider how to handle non-iid data at the different clients. One should also consider dynamic ways of partitioning the data based on changing conditions like network bandwidth or availability or resource availability on each device.

REFERENCES

- [1] J. Deng, W. Dong, R. Socher, L.-J. Li, K. Li, and L. Fei-Fei, "Imagenet: A large-scale hierarchical image database," in *2009 IEEE conference on computer vision and pattern recognition*. Ieee, 2009, pp. 248–255.
- [2] O. Yurur, C. H. Liu, and W. Moreno, "A survey of context-aware middleware designs for human activity recognition," *IEEE Communications Magazine*, vol. 52, no. 6, pp. 24–31, 2014.
- [3] S. Ranasinghe, F. Al Machot, and H. C. Mayr, "A review on applications of activity recognition systems with regard to performance and evaluation," *International Journal of Distributed Sensor Networks*, vol. 12, no. 8, p. 1550147716665520, 2016.
- [4] R. Girdhar, D. Ramanan, A. Gupta, J. Sivic, and B. Russell, "Actionvlad: Learning spatio-temporal aggregation for action classification," in *Proceedings of the IEEE Conference on Computer Vision and Pattern Recognition*, 2017, pp. 971–980.
- [5] J. Carreira and A. Zisserman, "Quo vadis, action recognition? a new model and the kinetics dataset," in *proceedings of the IEEE Conference on Computer Vision and Pattern Recognition*, 2017, pp. 6299–6308.
- [6] A. Diba, M. Fayyaz, V. Sharma, A. Hossein Karami, M. Mahdi Arzani, R. Yousefzadeh, and L. Van Gool, "Temporal 3d convnets using temporal transition layer," in *Proceedings of the IEEE Conference on Computer Vision and Pattern Recognition Workshops*, 2018, pp. 1117–1121.
- [7] R. Girdhar, J. Carreira, C. Doersch, and A. Zisserman, "Video action transformer network," in *Proceedings of the IEEE/CVF Conference on Computer Vision and Pattern Recognition*, 2019, pp. 244–253.
- [8] H. Zhang, L. Zhang, X. Qi, H. Li, P. H. Torr, and P. Koniusz, "Few-shot action recognition with permutation-invariant attention," in *Proceedings of the European Conference on Computer Vision (ECCV)*. Springer, 2020.
- [9] S. Kumar Dwivedi, V. Gupta, R. Mitra, S. Ahmed, and A. Jain, "Protogan: Towards few shot learning for action recognition," in *Proceedings of the IEEE/CVF International Conference on Computer Vision Workshops*, 2019, pp. 0–0.
- [10] B. Brattoli, J. Tighe, F. Zhdanov, P. Perona, and K. Chalupka, "Re-thinking zero-shot video classification: End-to-end training for realistic applications," in *Proceedings of the IEEE/CVF Conference on Computer Vision and Pattern Recognition*, 2020, pp. 4613–4623.
- [11] D. Mandal, S. Narayan, S. K. Dwivedi, V. Gupta, S. Ahmed, F. S. Khan, and L. Shao, "Out-of-distribution detection for generalized zero-shot action recognition," in *Proceedings of the IEEE/CVF Conference on Computer Vision and Pattern Recognition*, 2019, pp. 9985–9993.
- [12] W. Kay, J. Carreira, K. Simonyan, B. Zhang, C. Hillier, S. Vijayanarasimhan, F. Viola, T. Green, T. Back, P. Natsev *et al.*, "The kinetics human action video dataset," *arXiv preprint arXiv:1705.06950*, 2017.
- [13] H. Kuehne, H. Jhuang, E. Garrote, T. Poggio, and T. Serre, "Hmdb: a large video database for human motion recognition," in *2011 International conference on computer vision*. IEEE, 2011, pp. 2556–2563.
- [14] K. Soomro, A. R. Zamir, and M. Shah, "Ucf101: A dataset of 101 human actions classes from videos in the wild," *arXiv preprint arXiv:1212.0402*, 2012.
- [15] K. Hara, H. Kataoka, and Y. Satoh, "Learning spatio-temporal features with 3d residual networks for action recognition," in *Proceedings of the IEEE International Conference on Computer Vision Workshops*, 2017, pp. 3154–3160.
- [16] —, "Can spatiotemporal 3d cnns retrace the history of 2d cnns and imagenet?" in *Proceedings of the IEEE conference on Computer Vision and Pattern Recognition*, 2018, pp. 6546–6555.

- [17] M. Li, E. Yumer, and D. Ramanan, "Budgeted training: Rethinking deep neural network training under resource constraints," *arXiv preprint arXiv:1905.04753*, 2019.
- [18] K. Bonawitz, H. Eichner, W. Grieskamp, D. Huba, A. Ingerman, V. Ivanov, C. Kiddon, J. Konečný, S. Mazzocchi, H. B. McMahan *et al.*, "Towards federated learning at scale: System design," *arXiv preprint arXiv:1902.01046*, 2019.
- [19] X. Feng, Y. Jiang, X. Yang, M. Du, and X. Li, "Computer vision algorithms and hardware implementations: A survey," *Integration*, vol. 69, pp. 309–320, 2019.
- [20] K. Bonawitz, V. Ivanov, B. Kreuter, A. Marcedone, H. B. McMahan, S. Patel, D. Ramage, A. Segal, and K. Seth, "Practical secure aggregation for privacy-preserving machine learning," in *proceedings of the 2017 ACM SIGSAC Conference on Computer and Communications Security*, 2017, pp. 1175–1191.
- [21] P. Blanchard, E. M. El Mhamdi, R. Guerraoui, and J. Stainer, "Machine learning with adversaries: Byzantine tolerant gradient descent," in *Proceedings of the 31st International Conference on Neural Information Processing Systems*, 2017, pp. 118–128.
- [22] G. Xu, H. Li, S. Liu, K. Yang, and X. Lin, "Verifynet: Secure and verifiable federated learning," *IEEE Transactions on Information Forensics and Security*, vol. 15, pp. 911–926, 2019.
- [23] V. Mugunthan, A. Peraire-Bueno, and L. Kagal, "Privacyfl: A simulator for privacy-preserving and secure federated learning," in *Proceedings of the 29th ACM International Conference on Information & Knowledge Management*, 2020, pp. 3085–3092.
- [24] Z. Chai, H. Fayyaz, Z. Fayyaz, A. Anwar, Y. Zhou, N. Baracaldo, H. Ludwig, and Y. Cheng, "Towards taming the resource and data heterogeneity in federated learning," in *2019 {USENIX} Conference on Operational Machine Learning (OpML 19)*, 2019, pp. 19–21.
- [25] Z. Chai, A. Ali, S. Zawad, S. Truex, A. Anwar, N. Baracaldo, Y. Zhou, H. Ludwig, F. Yan, and Y. Cheng, "Tiff: A tier-based federated learning system," in *Proceedings of the 29th International Symposium on High-Performance Parallel and Distributed Computing*, 2020, pp. 125–136.
- [26] C. Xie, S. Koyejo, and I. Gupta, "Asynchronous federated optimization," *arXiv preprint arXiv:1903.03934*, 2019.
- [27] G. Hinton, O. Vinyals, and J. Dean, "Distilling the knowledge in a neural network," *NIPS 2014 Deep Learning Workshop*, 2015.
- [28] S. I. Mirzadeh, M. Farajtabar, A. Li, N. Levine, A. Matsukawa, and H. Ghasemzadeh, "Improved knowledge distillation via teacher assistant," in *Proceedings of the AAAI Conference on Artificial Intelligence*, vol. 34, no. 04, 2020, pp. 5191–5198.
- [29] Y. Liu, A. Huang, Y. Luo, H. Huang, Y. Liu, Y. Chen, L. Feng, T. Chen, H. Yu, and Q. Yang, "Fedvision: An online visual object detection platform powered by federated learning," in *Proceedings of the AAAI Conference on Artificial Intelligence*, vol. 34, no. 08, 2020, pp. 13 172–13 179.
- [30] B. McMahan, E. Moore, D. Ramage, S. Hampson, and B. A. y Arcas, "Communication-efficient learning of deep networks from decentralized data," in *Artificial Intelligence and Statistics*. PMLR, 2017, pp. 1273–1282.
- [31] P. Yu and Y. Liu, "Federated object detection: Optimizing object detection model with federated learning," in *Proceedings of the 3rd International Conference on Vision, Image and Signal Processing*, 2019, pp. 1–6.
- [32] G. A. Kaissis, M. R. Makowski, D. Rückert, and R. F. Braren, "Secure, privacy-preserving and federated machine learning in medical imaging," *Nature Machine Intelligence*, vol. 2, no. 6, pp. 305–311, 2020.
- [33] E. Jeong, S. Oh, H. Kim, J. Park, M. Bennis, and S.-L. Kim, "Communication-efficient on-device machine learning: Federated distillation and augmentation under non-iid private data," *arXiv preprint arXiv:1811.11479*, 2018.
- [34] R. Anil, G. Pereyra, A. Passos, R. Ormandi, G. E. Dahl, and G. E. Hinton, "Large scale distributed neural network training through online distillation," *arXiv preprint arXiv:1804.03235*, 2018.
- [35] Y. LeCun, L. Bottou, Y. Bengio, and P. Haffner, "Gradient-based learning applied to document recognition," *Proceedings of the IEEE*, vol. 86, no. 11, pp. 2278–2324, 1998.
- [36] K. Sozinov, V. Vlassov, and S. Girdzijauskas, "Human activity recognition using federated learning," in *2018 IEEE Intl Conf on Parallel & Distributed Processing with Applications, Ubiquitous Computing & Communications, Big Data & Cloud Computing, Social Computing & Networking, Sustainable Computing & Communications (ISPA/IUCC/BDCloud/SocialCom/SustainCom)*. IEEE, 2018, pp. 1103–1111.
- [37] S. Ek, F. Portet, P. Lalanda, and G. Vega, "Evaluation of federated learning aggregation algorithms: application to human activity recognition," in *Adjunct Proceedings of the 2020 ACM International Joint Conference on Pervasive and Ubiquitous Computing and Proceedings of the 2020 ACM International Symposium on Wearable Computers*, 2020, pp. 638–643.
- [38] S. Wang, T. Tuor, T. Salonidis, K. K. Leung, C. Makaya, T. He, and K. Chan, "Adaptive federated learning in resource constrained edge computing systems," *IEEE Journal on Selected Areas in Communications*, vol. 37, no. 6, pp. 1205–1221, 2019.
- [39] W. Y. B. Lim, N. C. Luong, D. T. Hoang, Y. Jiao, Y.-C. Liang, Q. Yang, D. Niyato, and C. Miao, "Federated learning in mobile edge networks: A comprehensive survey," *IEEE Communications Surveys & Tutorials*, vol. 22, no. 3, pp. 2031–2063, 2020.
- [40] Z. Xu, Z. Yang, J. Xiong, J. Yang, and X. Chen, "Elfish: Resource-aware federated learning on heterogeneous edge devices," *arXiv preprint arXiv:1912.01684*, 2019.
- [41] Y. Chen, Y. Ning, M. Slawski, and H. Rangwala, "Asynchronous online federated learning for edge devices with non-iid data," *arXiv preprint arXiv:1911.02134*, 2019.
- [42] S. Y. Nikouei, Y. Chen, S. Song, R. Xu, B.-Y. Choi, and T. Faughnan, "Smart surveillance as an edge network service: From harr-cascade, svm to a lightweight cnn," in *2018 IEEE 4th International Conference on Collaboration and Internet Computing (CIC)*. IEEE, 2018, pp. 256–265.
- [43] Z. Q. Lin, A. G. Chung, and A. Wong, "Edgespeechnets: Highly efficient deep neural networks for speech recognition on the edge," *arXiv preprint arXiv:1810.08559*, 2018.
- [44] A. Reisizadeh, A. Mokhtari, H. Hassani, A. Jadbabaie, and R. Pedarsani, "Fedpaq: A communication-efficient federated learning method with periodic averaging and quantization," in *International Conference on Artificial Intelligence and Statistics*. PMLR, 2020, pp. 2021–2031.
- [45] F. Sattler, S. Wiedemann, K.-R. Müller, and W. Samek, "Robust and communication-efficient federated learning from non-iid data," *IEEE transactions on neural networks and learning systems*, vol. 31, no. 9, pp. 3400–3413, 2019.
- [46] J. Mills, J. Hu, and G. Min, "Communication-efficient federated learning for wireless edge intelligence in iot," *IEEE Internet of Things Journal*, vol. 7, no. 7, pp. 5986–5994, 2019.
- [47] V. Smith, C.-K. Chiang, M. Sanjabi, and A. Talwalkar, "Federated multi-task learning," in *Proceedings of the 31st International Conference on Neural Information Processing Systems (NeurIPS)*, 2017, pp. 4427–4437.
- [48] X. Zhang, X. Zhou, M. Lin, and J. Sun, "Shufflenet: An extremely efficient convolutional neural network for mobile devices," in *Proceedings of the IEEE conference on computer vision and pattern recognition*, 2018, pp. 6848–6856.
- [49] B. Wu, X. Dai, P. Zhang, Y. Wang, F. Sun, Y. Wu, Y. Tian, P. Vajda, Y. Jia, and K. Keutzer, "Fbnet: Hardware-aware efficient convnet design via differentiable neural architecture search," in *Proceedings of the IEEE/CVF Conference on Computer Vision and Pattern Recognition*, 2019, pp. 10 734–10 742.
- [50] K. Han, Y. Wang, Q. Tian, J. Guo, C. Xu, and C. Xu, "Ghostnet: More features from cheap operations," in *Proceedings of the IEEE/CVF Conference on Computer Vision and Pattern Recognition*, 2020, pp. 1580–1589.
- [51] I. Jang, H. Kim, D. Lee, Y.-S. Son, and S. Kim, "Knowledge transfer for on-device deep reinforcement learning in resource constrained edge computing systems," *IEEE Access*, vol. 8, pp. 146 588–146 597, 2020.
- [52] Y. Matsubara, D. Callegaro, S. Baidya, M. Levorato, and S. Singh, "Head network distillation: Splitting distilled deep neural networks for resource-constrained edge computing systems," *IEEE Access*, vol. 8, pp. 212 177–212 193, 2020.
- [53] T. He, C. Shen, Z. Tian, D. Gong, C. Sun, and Y. Yan, "Knowledge adaptation for efficient semantic segmentation," in *Proceedings of the IEEE/CVF Conference on Computer Vision and Pattern Recognition*, 2019, pp. 578–587.
- [54] Q. Liu, L. Xie, H. Wang, and A. L. Yuille, "Semantic-aware knowledge preservation for zero-shot sketch-based image retrieval," in *Proceedings of the IEEE/CVF International Conference on Computer Vision*, 2019, pp. 3662–3671.
- [55] Q. Xie, M.-T. Luong, E. Hovy, and Q. V. Le, "Self-training with noisy student improves imagenet classification," in *Proceedings of the IEEE/CVF Conference on Computer Vision and Pattern Recognition*, 2020, pp. 10 687–10 698.
- [56] F. M. Thoker and J. Gall, "Cross-modal knowledge distillation for action recognition," in *2019 IEEE International Conference on Image Processing (ICIP)*. IEEE, 2019, pp. 6–10.
- [57] K. He, X. Zhang, S. Ren, and J. Sun, "Deep residual learning for image recognition," in *Proceedings of the IEEE conference on computer vision and pattern recognition*, 2016, pp. 770–778.
- [58] M. Wang and W. Deng, "Deep visual domain adaptation: A survey," *Neurocomputing*, vol. 312, pp. 135–153, 2018.

- [59] S. Sun, Y. Cheng, Z. Gan, and J. Liu, "Patient knowledge distillation for bert model compression," in *Proceedings of the 2019 Conference on Empirical Methods in Natural Language Processing and the 9th International Joint Conference on Natural Language Processing (EMNLP-IJCNLP)*, 2019, pp. 4314–4323.
- [60] J. Liu, Y. Wang, and Y. Qiao, "Sparse deep transfer learning for convolutional neural network," in *Proceedings of the AAAI Conference on Artificial Intelligence*, vol. 31, no. 1, 2017.
- [61] M. E. Kalfaoglu, S. Kalkan, and A. A. Alatan, "Late temporal modeling in 3d cnn architectures with bert for action recognition," in *European Conference on Computer Vision*. Springer, 2020, pp. 731–747.